Chapter 11

Flexible Wings and Fluid–Structure Interactions for Micro-Air Vehicles

W. Shyy, Y. Lian, S.K. Chimakurthi, J. Tang, C.E.S. Cesnik, B. Stanford, and P.G. Ifju

Abstract Aerodynamics, structural dynamics, and flight dynamics of natural flyers intersect with some of the richest problems in micro-air vehicles (MAVs), including massively unsteady three-dimensional separation, transition in boundary and shear layers, vortical flows, unsteady flight environment, aeroelasticity, and adaptive control being just a few examples. A challenge is that the scaling of both fluid dynamics and structural dynamics between smaller natural flyer and practical flying hardware/lab experiment (larger dimension) is fundamentally difficult. The interplay between flexible structures and aerodynamics motivated by the MAV development is discussed in this chapter. For fixed wings, membrane materials exhibit self-initiated vibration even in a steady free stream which lowers the effective angle of attack of the membrane structure compared to that of the rigid wing. For flapping wings, structural flexibility can enhance leading-edge suction via increasing the effective angle of attack, resulting in higher thrust generation.

11.1 Introduction

Micro-air vehicles (MAVs) have the potential to revolutionize our capabilities of gathering information in environmental monitoring, homeland security, and other time-sensitive areas. To fulfill this potential, MAVs must have the ability to fly in urban settings, tunnels, and caves; maintain forward and hovering flight; maneuver in constrained environments, and "perch" until needed. Due to the MAVs' small size, flight regime, and modes of operation, significant scientific advancement will be needed to create this revolutionary capability. From a biology-inspired viewpoint, aerodynamics, structural dynamics, and flight dynamics of birds, bats, and insects intersect with some of the richest problems in aerospace engineering: massively unsteady three-dimensional separation, transition in boundary and shear layers, vortical flows, unsteady flight environment, aeroelasticity, and adaptive control being just a few examples.

Natural flyers have several outstanding features which may pose several challenges in the design of MAVs. For example, (i) there is substantial anisotropy in the wing structural characteristics between the chordwise and spanwise directions, (ii) they employ shape control to accommodate spatial and temporal flow structures, (iii) they accommodate wind gusts and accomplish station keeping with varying kinematics patterns, (iv) they utilize multiple unsteady aerodynamic mechanisms for lift and thrust enhancement, and (v) they combine sensing, control, and wing maneuvering to maintain not only lift but also flight stability. In principle, one might like to first understand these biological systems, abstract certain desirable features, and then apply them to MAV design. A challenge is that the scaling of both fluid dynamics and structural dynamics between smaller natural flyers and practical flying hardware/lab experiments (larger dimension) is fundamentally difficult. Regardless, in order to develop a satisfactory flyer, one needs to meet the following objectives:

W. Shyy (✉)
Department of Aerospace Engineering, University of Michigan, Ann Arbor, Michigan, USA
e-mail: weishyy@umich.edu

D. Floreano et al. (eds.), *Flying Insects and Robots*,
DOI 10.1007/978-3-540-89393-6_11, © Springer-Verlag Berlin Heidelberg 2009

- generate necessary lift, which scales with the vehicle/wing length scale as l^3(under geometric similitude); however, oftentimes, a flyer needs to increase or reduce lift to maneuver towards/avoid an object, resulting in the need for substantially more complicated considerations;
- minimize the power consumption.

An optimal design based on a single design point, under a given steady free stream value, is insufficient; instead, we need to develop a knowledge base guiding future design of MAVs across a range of wind gust, flight speed, and time scales so that they can be optimal flyers within the entire flight envelope.

When wind gust adjustment, object avoidance, or station keeping become major factors, highly deformed wing shapes and coordinated wing-tail movement are often observed. Figure 11.1a illustrates such behavior for a hummingbird maneuvering around a potential threat and a chickadee adjusting its flight path to accommodate a target. Understanding of the aerodynamic, structural, and control implications of these modes is essential for the development of high performance and robust micro-air vehicles capable of performing desirable missions. The large flexibility of animal wings leads to complex fluid–structure interactions, while the kinematics of flapping and the spectacular maneuvers performed by natural flyers result in highly coupled nonlinearities in fluid mechanics, aeroelasticity, flight dynamics, and control systems.

Furthermore, as already mentioned before, insect wing properties are anisotropic because of the membrane-batten structures, with the spanwise bending stiffness about 1 to 2 orders of magnitude larger than the chordwise bending stiffness in a majority of insect species. In general, spanwise flexural stiffness scales with the third power of the wing chord while the chordwise stiffness scales with the second power of the wing chord [5]. Figure 11.1b shows the wing of a dragonfly. It has a reinforced leading edge and local variations in structural composition in terms of corrugation, for example. It has been shown in literature that wing corrugation increases both warping rigidity and flexibility. Furthermore, specific characteristic features have been observed on the wing structure of a dragonfly which even help prevent fatigue fracture [27].

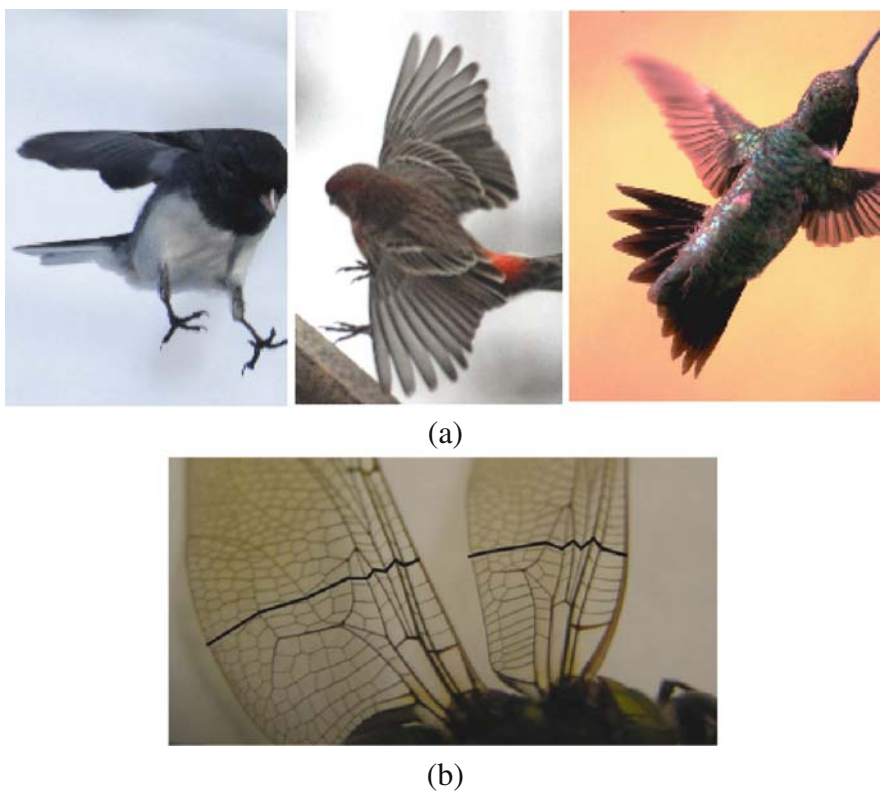

Fig. 11.1 (**a**) Asymmetric flapping kinematics, involving wing–tail coordination, are displayed with a hummingbird avoiding a potential threat and a nuthatch making adjustment while flying toward a target. (**b**) Wing structure of a dragonfly with reinforced leading-edge, anisotropic mechanical property distribution, and corrugated geometry

Moreover, the thin nature of the insect wing skin structure makes it unsuitable for taking compressive loads, which may result in skin wrinkling and/or buckling (i.e., large local deformations that will interact with the flow). Overall, insect wings have deformable aerofoils, whose instantaneous shape through the stroke cycle is determined, largely automatically, by the interaction of their structural elasticity and the inertial and aerodynamic forces they are experiencing [46]. On the aerodynamics side, in a fixed-wing setup, wind tunnel measurements show that corrugated wings are aerodynamically insensitive to the Reynolds number variations, which is quite different from a typical low Reynolds number airfoil.

Can large flexible deformations provide a better interaction with the aerodynamics than if limited to the linear regimes? If torsional stiffness along the wing span can be tailored, how can that affect the wing kinematics for optimum thrust generation? How do these geometrically nonlinear effects and the anisotropy of the structure impact the aerodynamics characteristics of the flapping wing? All of these are issues that require detailed investigations and the understanding of which is critical for the success of future MAV designs.

Due to the foregoing reasons and many others, fluid–structure interaction studies are critical to MAV design. Much of the efforts in this area thus far have focused on fixed-wing membrane-based vehicles [19, 29, 34, 36, 38]. Shyy et al. [28] have discussed flexible wings utilizing membrane materials and inferred from computations that compared to a rigid wing, a membrane wing can adapt to stall better and has the potential to achieve enhanced agility and storage condition by morphing its shape. They also emphasized the importance of fluid–structure analyses to understand the membrane wing performance. Lian and Shyy [19] have studied the three-dimensional interaction between a membrane wing and its surrounding fluid flow via an aeroelastic coupling of a nonlinear membrane structural solver and a Navier–Stokes solver. Stanford et al. [36] made a direct comparison of wing displacements, strains, and aerodynamic loads obtained via a novel experimental setup with those obtained numerically. In their work, they considered both pre- and post-stall angles of attack and the computed flow structures revealed several key aeroelastic effects: decreased tip vortex strength, pressure spikes and flow deceleration at the tangent discontinuity of the inflated membrane boundary, and an adaptive shift of pressure distribution in response to aerodynamic loading.

The aeroelasticity of flapping wings has only recently been seriously addressed and a full picture of the basic aeroelastic phenomena in flapping flight is still not clear [3, 4, 9, 13, 14, 22, 24, 28, 31–33, 39, 40, 44, 47]. For example, Frampton et al. [9] have investigated a method of wing construction that results in an optimal relationship between flapping wing bending and twisting such that optimal thrust forces are generated. The thrust production of flapping wings was tested in an experimental rig. Results from this study indicated that the phase between bending and torsional motion is critical for the production of thrust. It was noted that a wing with bending and torsional motion in phase creates the largest thrust whereas a wing with the torsional motion lagging the bending motion by 90° results in the best efficiency. Hamamoto et al. [13] have conducted finite element analysis based on the arbitrary Lagrangian–Eulerian method to perform fluid–structure interaction analysis on a deformable dragonfly wing in hover and examined the advantages and disadvantages of flexibility. They tested three types of flapping flight: a flexible wing driven by dragonfly flapping motion, a rigid wing (stiffened version of the original flexible dragonfly wing) driven by dragonfly flapping motion, and a rigid wing driven by modified flapping based on tip motion of the flexible wing. They found that the flexible wing with nearly the same average energy consumption generated almost the same amount of lift force as the rigid wing with modified flapping motion. In this case, the motion of the tip of the flexible wing provided equivalent lift as the motion of the root of the rigid wing. However, the rigid wing required 19% more peak torque and 34% more peak power, indicating the usefulness of wing flexibility. More recently, Singh [32] has discussed a computational framework for the aeroelastic analysis of hover-capable, bio-inspired flapping wings. The chord-based Reynolds number considered for the analyses was in the 10^3–10^5 range. One of the major inferences from this work is that at high flapping frequencies (12 Hz), the light-weight and highly flexible insect-like wings used in the study exhibited significant aeroelastic effects.

Zhu [47] has developed a nonlinear fluid–structure interaction approach to study the unsteady oscillation of a flexible wing. He found that when the wing is immersed in air, the chordwise flexibility reduces

both the thrust and the propulsion efficiency whereas spanwise flexibility (through equivalent plunge and pitch flexibility) increases the thrust without efficiency reduction within a small range of structural parameters. However, when the wing is immersed in water, the chordwise flexibility increased the efficiency and the spanwise flexibility reduced both the thrust and the efficiency. Wills et al. [44] have presented a computational framework to design and analyze flapping MAV flight. A series of different geometric and physical fidelity level representations of solution methodologies was described in the work. Liani et al. [22] have coupled an unsteady panel method with Lagrange's equations of motion for a two degree-of-freedom (2 DOF) spring-mass wing section system to investigate the aeroelastic effect on the aerodynamic forces produced by a flexible flapping wing at different frequencies especially near its resonance. Heathcote et al. [14] have experimentally investigated the effects of stiffness on thrust generation of airfoils undergoing a plunging motion under various free stream velocities. Direct force measurements showed that the thrust/input-power ratio was found to be greater for flexible airfoils than for the rigid one. They also observed that at high plunging frequencies, the less flexible airfoil generates the largest thrust, while the more flexible airfoil generates the most thrust at low frequencies. To study the effect of the spanwise stiffness on the thrust, lift, and propulsive efficiency of a plunging wing, a water tunnel study was conducted on a NACA0012 uniform wing of aspect ratio 3. They observed that, for Strouhal numbers greater than 0.2, a degree of spanwise flexibility was found to be beneficial. Tang et al. [40] explored a two-dimensional flexible airfoil by coupling a pressure-based fluid solver with a linear beam solver. In this work, the fluid flow around a plate of different thicknesses with a teardrop-shaped leading edge was computed at a Reynolds number of 9×10^3. In addition to this, a flat plate with half-cylinders at leading and trailing edges were investigated at a Reynolds number of 10^2 to probe the mechanism of thrust generation. In particular, they pointed out that the effect of the deformation (passive pitching) is similar to the rigid body motion (rigid pitching), meaning that the detailed shape of the airfoil is secondary to the equivalent angle of attack.

In contrast to the aforementioned studies, [6] explored the relative contributions of inertial-elastic and fluid dynamic forces by oscillating Manduca wings at 25 Hz in both normal air and helium. In the paper, the authors show that the overall wing motions and bending patterns are quite similar in both the cases, despite the 85% reduction in fluid density in the case of helium, suggesting that the contribution of aerodynamic forces are relatively small compared to the contribution of inertial-elastic processes. It was then suggested that, for studies of animal flight in air the somewhat intractable problem of fluid–solid coupling in wing design does not need to be addressed. In this connection, [42] suggested that, unfortunately, the inherent challenge of obtaining flowfield measurements in the wake of a living insect makes such postulations difficult to test and that such conclusions are often based on simple models for the aerodynamic forces that generally neglect much of the important unsteady fluid dynamics.

This chapter presents a perspective regarding the issues, progress, and challenges associated with unsteady low Reynolds number aerodynamics associated with wing flexibility and their implications on micro-air vehicles. The parameters considered in the model problems presented here are general and do not target any particular insect.

11.2 Parameter Space and Scaling Laws

From the viewpoint of fluid and structural dynamics, there are different dimensionless parameters that are of relevance to our study. Consider c, chord length; ω, circular frequency of flapping (rad/s); h_a, flapping amplitude; U_{ref}, reference velocity; ν, kinematic viscosity; ρ_f, fluid density; D, plate stiffness (directly proportional to material Young's modulus and the cube of the wing thickness); I_B, (flapping) moment of inertia; ω_B and ω_T being wing linear natural frequencies of bending and torsion, respectively. The relevant dimensionless parameters are listed in Table 11.1. Assuming that the geometric similarity is maintained, the scaling laws for forward and hovering flight conditions are summarized in the same table. One can readily conclude that the hovering Reynolds number and the cruising Reynolds number are very close to each other because the characteristic velocity for hovering is $U_{ref} = \omega h_a$. For hovering, the reduced frequency becomes $k = c/2h_a$, which is simply related to the normalized stroke amplitude. Furthermore, if

Table 11.1 Dimensionless parameters and scaling dependency for flapping wings

Dimensionless parameter	Hovering		Forward flight	
	Based on flapping wing speed		Based on cruising speed	
Reynolds number: $Re = \frac{U_{ref}c}{\nu}$	l^2	f	l	Independent
[1]Strouhal number: $St = \frac{\omega h_a}{\pi U_{ref}}$	Independent	Independent	l	f
Reduced frequency: $k = \frac{\pi \omega c}{2\pi U_{ref}}$	Independent	Independent	l	f
[2]$\Pi_1 = \frac{D}{\rho_f U_{ref}^2 c^3}$	l^{-2}	f^{-2}	Independent	Independent
[3]$\Pi_2 = \frac{I_B}{\rho_f c^5}$	l^{-1}	Independent	l^{-1}	Independent
[4]$\Pi_3 = \frac{\omega_B}{\omega}$	l^{-1}	f^{-1}	l^{-1}	f^{-1}
[5]$\Pi_4 = \frac{\omega_T}{\omega}$	l^{-1}	f^{-1}	l^{-1}	f^{-1}

[1]It is noted that the advance ratio $J = U_{ref}/(\omega h_a)$ is related to St, specifically $J = 1/(\pi St)$.
[2]Ratio of elastic and aerodynamic forces. Π_1 gives a relative measure of elastic deformation to given aerodynamic loading and it is important as a measure of the structural nonlinear regime. Π_1 is also related to the Kussner factor for flutter estimation. The applicability of the latter to the flapping wing stability boundary is uncertain however, and this should be investigated.
[3]Ratio of inertia and aerodynamic generalized forces. Π_2 is related to the Lock number and it contains the mass ratio (representing the relative density of the wing and the fluid surrounding it).
[4]Ratio of first linear bending natural frequency [23] and the frequency of excitation.
[5]Ratio of first linear torsion natural frequency [23] and the frequency of excitation.

we use the forward flight speed as the velocity scale, the resulting non-dimensional form of the momentum equation explicitly contains the Reynolds number and the Strouhal number. On the other hand, if we choose to use the flapping velocity scale, then the momentum equation will explicitly contain the Reynolds number and the reduced frequency [30]. As shown in Table 11.1, the scaling laws make the construction of aeroelastic models and testing complicated. Moreover, it leads to the usage of structural materials with elastic properties that are different from those of the structure of the natural flyer. Table 11.2 shows selected structural and flow properties of three low Re flyers. Table 11.3 shows several dimensionless parameters for the three low Re flyers listed in Table 11.2. For the calculation of the plate stiffness in Π_1, Young's modulus information along the span was considered. Specifications for the humming bird were obtained from [7], whereas those for the bumblebee and hawkmoth were obtained from Fig. 11.4 of [5]. It may be noted that in the calculation of the dimensionless parameters Π_3 and Π_4, the wing was assumed to be a beam with a

Table 11.2 Selected structural and flow properties of three low Re flyers

Insect	Mean chord length c (cm)	Wing mass (mg)	Forward velocity (U in m/s)	Mean wing thickness (cm)	Wing semi span (cm)
Bumblebee	0.4	0.45	4.5	7×10^{-4}	1.3
Hawkmoth	1.8	47	5	3.4×10^{-3}	4.9
Hummingbird	2.0	294	8	0.1	8.5

Table 11.3 Dimensionless parameters for the low Re flyers listed in Table 11.2

Parameter	BumbleBee	Hawkmoth	Hummingbird
AR	6.6	5.3	8.2
R_e	1.2×10^3–3×10^3	4.2×10^3–5.3×10^3	1.1×10^4
St	0.48	0.35	0.93
k	0.23	0.3	0.15
Π_1	510	61	1.56×10^3
Π_2	20	12.7	170
Π_3	6.5	4.6	7.9
Π_4	1.1×10^2	62	61

rectangular cross section whose length is equal to the mean chord and breadth to the mean thickness of the wing.

11.3 Fixed Membrane Wing MAVs

Nature's design of flexible membrane wings can be put into practice for MAVs. The membrane concept has been successfully incorporated in MAVs designed by Ifju et al. [16]. In their design illustrated in Fig. 11.2, unidirectional carbon fiber and cloth prepreg materials have been used for the skeleton (leading-edge spar and chordwise battens) and latex rubber sheet material for the membrane. The stiffness of the whole structure can be controlled by the number of battens and membrane material in such a construction.

Passive shape adaptation can be built into such a membrane wing via its interaction with aerodynamic loading through either geometric or aerodynamic twist [30, 35]. Its successful implementation is particularly important for micro-air vehicles beset with several flight issues: poor wing efficiency due to separation of the low Reynolds number flow, rolling instabilities, bilateral asymmetries due to destabilization of the low aspect ratio wing's tip vortices, and wind gusts of the same order of magnitude as the original flight speed. The dynamic membrane model computations by Lian [18] and Lian et al. [21] have shown that even in steady free stream, the membrane wing experienced high-frequency vibrations. Navier–Stokes simulations and experimental studies report that, for membrane-type flexible structures under typical MAV Reynolds numbers, the structural response is around O(100) Hz [31]. These issues, along with stable weight management and flight control problems that intensify with decreasing vehicle sizes, can be potentially attenuated with proper load redistribution over the wing.

Fig. 11.2 Six-inch flexible, fixed-wing MAV [16]

In an attempt to understand the aerodynamics/aeroelasticity aspects of membrane wings, in [30, 35], a rigid wing and two flexible, fixed-wing MAV structures were considered. The first of the latter two had membrane wings with several chordwise batten structures and a free trailing edge for geometric twist (batten-reinforced wings, BR). And the second had membrane wings whose interior is unconstrained and is sealed along the perimeter to a stiff laminate for aerodynamic twist (perimeter-reinforced wings, PR). Typical flow structures for all three wings are shown in Fig. 11.3, for 15° angle of attack (α) and 15 m/s free stream velocity (U_∞). The two predominant hallmarks of MAV aerodynamics can be seen from the flow over the rigid wing: the low Reynolds number (10^5) causes the laminar boundary layer to separate against the adverse pressure gradient at the wing root, and the low aspect ratio (1.2) forces a strong wing tip vortex swirling system and leaves a low-pressure region at the wing tip.

Flow over the flexible BR wing is characterized by pressure undulations over the surface [15], where the membrane inflation between each batten re-directs the flow. The shape adaptation decreases the strength of the adverse pressure gradient, and thus the size of the separation bubble. A large pressure spike develops over the PR wing at the leading edge of the membrane skin. The pressure recovery over the wing is shifted aftward, and flow separates as it travels down the inflated shape, where it is then entrained into the low-pressure core of the tip vortex. This interaction between the tip vortices and the longitudinal flow separation is known to lead to unsteady vortex destabilization at high angles of attack [41]; no such relationship is obvious for the BR and rigid wings. The low-pressure regions at the wing tips of the two membrane wings are weaker than those observed on the rigid wing, presumably due to energy considerations: strain energy in the membrane may remove energy from the lateral swirling system. Furthermore, the inflated membrane shape may act as a barrier to the tip vortex formation.

The lift, drag, and pitching moment coefficients for the three different wings discussed above through

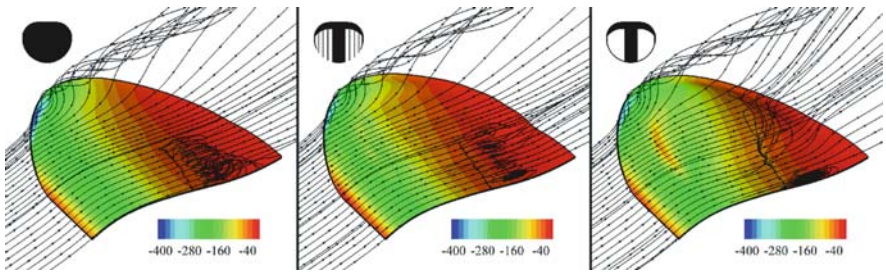

Fig. 11.3 Streamlines and pressure distributions (Pa) over the top wing surface: $\alpha = 15°$, $U_\infty = 15$ m/s [16]

an α-sweep are shown in Fig. 11.4. The $C_L - \alpha$ relationships are mildly nonlinear (20–25% increase in $C_{L\alpha}$ between 0° and 15°, $C_{L\alpha}$ is the lift curve slope) due to growth of the low-pressure cells at the wing tip. Further characteristics of a low aspect ratio are given by the high stall angle, computed as being 21° for the rigid case. The aerodynamic twist of the PR wing increases $C_{L\alpha}$ (by as much as 8%), making the MAV more susceptible to gusty conditions. C_{Lmax} is slightly higher as well, subsequently lowering the stall angle to 18°. The adaptive washout of the BR wing decreases $C_{L\alpha}$ (by as much as 15% over that of the rigid wing), though the change is negligible at lower angles of attack. This is thought to be a result of two offsetting factors: the adaptive washout at the trailing edge decreases the lift, while the inflation of the membrane toward the leading edge increases the effective camber, and hence the lift.

Also, comparing the drag polars of Fig. 11.4, it can be seen that both flexible wings incur a drag penalty at small lift values, indicative of the aerodynamically non-optimal shapes assumed by the flexible wings (though the BR wing has less drag at a given angle of attack [2]). The drag difference between the rigid and BR wing is very small, while the PR wing displays a larger penalty. This is presumably due to two factors: a greater percentage of the wing experiences flow separation, and a large portion of the pressure spike at the leading edge is pointed in the axial direction. Pitching moments (measured about the leading edge) have a negative slope with both C_L and α, as necessitated by stability requirements. Nonlinear trends due to low aspect ratio affects are again evident. Both the BR and the PR wings have a lower $\partial Cm/\partial C_L$ than the rigid wing, though only the PR wing shows a drastic change (by as much as 15%). This is a result of the membrane

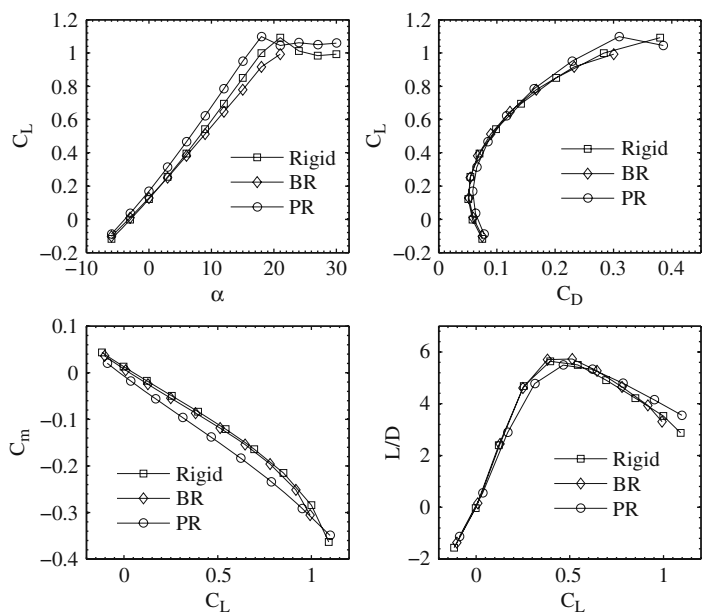

Fig. 11.4 Computed aerodynamic performance: $\alpha = 15°$, $U_\infty = 15$ m/s

inflation, which shifts the pressure recovery toward the trailing edge, adaptively increasing the strength of the restoring pitching moment with increases in lift or α [36].

Steeper C_m slopes indicate larger static margins: stability concerns are a primary target of design improvement from one generation of micro-air vehicles to the next. The range of flyable CG locations is generally only a few millimeters long; meeting this requirement represents a strenuous weight management challenge. Furthermore, the PR wing displays a greater range of linear C_m behavior, possibly due to the fact that the adaptive membrane inflation quells the strength of the low-pressure cells, as discussed above. No major differences appear between the L/D characteristics of the three wings for low angles of attack. At moderate angles, the large drag penalty of the PR wing decreases the efficiency, while the BR wing slightly out-performs the rigid wing. At higher angles, both the lift and drag characteristics of the PR wing are superior to the other two, resulting in the best L/D ratios.

Aeroelastic tailoring conventionally utilizes unbalanced laminates for bend/twist coupling, but the pre-tension within the membrane skin has an enormous impact on the aerodynamics: for the two-dimensional case, higher pre-tension generally pushes flexible wing performance to that of a rigid wing. For a three-dimensional wing, the response can be considerably more complex, depending on the nature of the membrane reinforcement. Effects of increasing the membrane pre-tension may include decrease in drag, decrease in $C_{L\alpha}$, linearized lift behavior, increase in the zero-lift angle of attack, and more abrupt stalling patterns. Furthermore, aeroelastic instabilities pertaining to shape hysteresis at low angles of attack can be avoided with specific ratios of spanwise-to-chordwise pre-tensions [25].

Increasing the pre-stress within the membrane skin of a BR wing (see [37]) generally increases $C_{L\alpha}$, decreases $C_{m\alpha}$ (slope of the moment curve), and decreases L/D. The system is very sensitive to changes in the pre-stress normal to the battens, and less so to the stress parallel to the battens, due to the zero-pre-stress condition at the free edge. Minimizing $C_{L\alpha}$ (for optimal gust rejection) is found with no pre-stress in the span direction and a mild amount in the chord direction. The unconstrained trailing edge eliminates the stiffness in this area (allowing for adaptive washout), but retains the stiffness toward the leading edge, removing the inflation seen here (and the corresponding increase in lift). Such a tactic reduces the conflicting sources of aeroelastic lift seen in a BR wing. Maximizing $C_{L\alpha}$ (for effective pull-up maneuvers, for example) is obtained by maximizing N_y and setting N_x to zero. Conversely, maximizing $C_{L\alpha}$ with a constraint on L/D might be obtained by maximizing N_x and setting N_y to zero.

Opposite trends are seen for a PR wing. Increasing the pre-stress within the membrane skin generally decreases $C_{L\alpha}$, increases $C_{m\alpha}$, and increases L/D. The chord-wise pre-stress has a negligible effect upon the stability derivatives, though both directions contribute equally to an improvement in L/D. As such, optimization of either derivative with a constraint on L/D could easily be provided by a design with maximum chord-wise pre-tension and a slack membrane in the span direction. Overall sensitivity of the aerodynamics to the pre-tension in the membrane skin of a BR or a PR wing can be large for the derivatives (up to a 20% change in the $C_{m\alpha}$ of a BR wing), though less so for the wing efficiency. Variations in L/D are never more than 5%.

Laminar-turbulent transition can affect the aerodynamic performance of MAVs flying at Reynolds numbers (10^4–10^5). In their study, Lian and Shyy [20] have performed numerical investigations to examine the impact of flexible surfaces on the transition process. For this, a Navier–Stokes solver, the e^N transition model, and a dynamic membrane model were coupled to study fluid–structure interaction. In the studied test case, a portion of the upper surface of the SD7003 airfoil was covered with a latex membrane that extends from 33 to 52% of the chord. No pre-tension was applied to the membrane. The membrane has a uniform thickness of 0.2 mm with a density of $1200\,\mathrm{kg/m^3}$. The reference scales of their computations are based on the free stream velocity of 0.3 m/s, density of $1000\,\mathrm{kg/m^3}$, and airfoil chord length of 0.2 m. With these parameters, the time step for the CFD solver here was set to 2×10^{-3} s and the time step of the structural solver was set to 1×10^{-5}s. In their work, subiterations between the CFD and the structural solver were used within each time step to allow for synchronization of the flow and the structure. By doing so, the errors introduced by a lagged fluid/structure coupling approach were regulated.

A computational test was performed at $\alpha = 4^\circ$ and $\mathrm{Re} = 6 \times 10^4$. It was observed that when flow passes

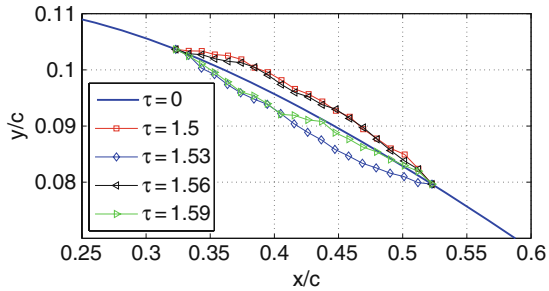

Fig. 11.5 Membrane airfoil shapes in a steady free stream at several time instants. The vibration changes the effective wing camber. τ is the non-dimensional time defined as tc/U [20]

over the flexible surface, the latter experiences self-excited oscillation and the airfoil displays a varied shape over time (Fig. 11.5). Analysis showed that the transverse velocity magnitude could reach as much as 10% of the free stream speed. During the vibration, energy was transferred from the wall to the flow and the separated flow was energized. Compared to the corresponding rigid airfoil simulation, the surface vibration caused both the separation and transition positions to exhibit a standard variation of 6% of its mean.

The time history of the lift coefficient for both the rigid and the membrane wings along with the time-averaged component for the latter are presented in [20]. Even though the time-averaged lift coefficient (0.60) of the flexible wing is comparable to that of the corresponding rigid wing, the lift coefficient displays a time-dependent variation with maximum magnitude that is as much as 15% of its mean. The drag coefficient shows a similar pattern, but the time-averaged value closely matches that of the rigid wing. The flexible wing, on the other hand, can delay the stall margin substantially [11, 43]. The FFT (fast Fourier transform) of the flexible wing response showed a dominant frequency at 167 Hz. Given the airfoil chord (0.2 m) and free stream speed (0.3 m/s), this high-vibration frequency is not likely to affect the vehicle stability. The time response of the lift coefficient indicates that a low-frequency component is present in the lift coefficient response along with the primary one. This component has a frequency of about 14 Hz and seems to be associated with the vortex shedding. In a different simulation with three-dimensional laminar flow over a 6 in. membrane wing (i.e., the entire wing surface is flexible), Lian and Shyy have observed a self-excited structural vibration with a frequency around 120 Hz [19]; the experimental measurement of similar wings recorded a primary frequency around 140 Hz [43].

In a different study, Lian et al. [21] have reviewed the aerodynamics of membrane and corresponding rigid wings under MAV flight conditions. Their numerical findings show that both membrane and rigid wings exhibit comparable aerodynamic performance before stall limit, which has also been experimentally observed by Waszak et al. [43]. Figure 11.6 shows the time-averaged vertical displacement of the trailing edge of the membrane wing at a free stream velocity of 10 m/s while the root chord Reynolds number is 9×10^4. The x-axis has the normalized distance of a point on the membrane (from the leading edge) with respect to the length of the membrane. The displacement is normalized with respect to the maximum camber of the wing and is shown on the y-axis in Fig. 11.6a. Due to the membrane deformation, the effective angle of attack (defined as the angle between the free stream velocity vector and the line joining

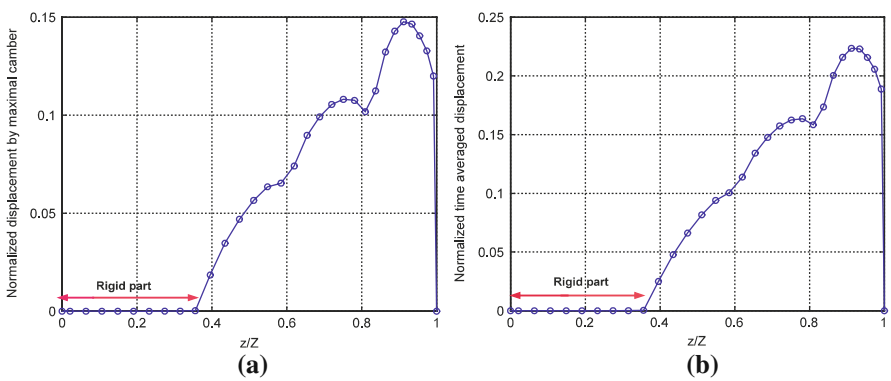

Fig. 11.6 Averaged displacement of the membrane wing trailing edge. (**a**) $\alpha = 6°$; (**b**) $\alpha = 15°$ [21]

the leading and trailing edge points at a station along the span) of the membrane wing is less than that of the rigid wing. The reduced effective angle of attack causes the decrease in the lift force in the case of the membrane wing.

11.4 Aeroelasticity of Flapping (Plunging) Wings

Flapping wing aircraft configurations received substantial attention up to early decades of the last century, though the aerodynamic and mechanical complexity of designing a flapping wing aircraft soon discouraged inventors. Furthermore, flapping wing vehicles are suitable only as flyer sizes become sufficiently small. The recently risen interest for a power-efficient MAV platform that is highly maneuverable and capable of low-speed flight with a stable hover and vertical take-off has re-ignited research and development efforts in flapping wing vehicles. High-speed cine and still photography and stroboscopy indicate that most biological flyers undergo orderly deformation in flight [45]. Birds, bats, and insects exploit the coupling between flexible wings and aerodynamic forces such that the wing deformations improve aerodynamic performance [9]. The interaction between unsteady aerodynamics and structural flexibility is, therefore, of considerable importance for MAV development.

Wing propulsion, which is a key issue in the study of flapping MAVs, has been widely investigated by several researchers in the past [1, 8, 10, 12, 17, 26] focusing on rigid structures. However, the impact of flexibility on flapping wing propulsion of three-dimensional wing structures in a low Reynolds number environment (10^4 to 10^5) is still not very well understood and needs more examination.

As part of validation efforts of a computational aeroelasticity framework that is suitable for flapping wing MAVs, [4] presented a fluid–structure coupling procedure between a Navier–Stokes solver and a quasi-three-dimensional finite element solver. Further, results were presented on a model example problem corresponding to a NACA0012 rectangular wing of aspect ratio 3 in pure heave motion at a Reynolds number of 3×10^4 for comparison to the experimental data of [14].

In their study, the wing structure was modeled as a one-dimensional beam with six elastic degrees of freedom, corresponding to extension, twist, and shear and bending in two directions. This choice was justified since the chordwise deformation was reported as being negligible in the experiment [14]. The wing cross section is built up from both PDMS (polydimethylsiloxane, which is a silicon-based organic polymer) and stainless steel. The mass and stiffness properties of the PDMS were not considered here; therefore, only the stainless steel stiffener (rectangular thin strip) was used for the evaluation of cross-sectional properties. The flapping axis was chosen at the leading-edge and the cross-sectional properties were evaluated with respect to the leading-edge point. Furthermore, the properties are uniform throughout the semi-span. A sinusoidal plunge profile as shown in Fig. 11.7 was prescribed to the root of the wing at the leading edge. The three-dimensional structural solution is obtained by using 75 recovery nodes on each cross section, resulting in a structured grid of 3000 interface points which define the solid side of the aeroelastic interface.

For the CFD analysis, a structured multi-block O-type grid around a NACA0012 wing of aspect ratio 3 was used. The number of grid points is 120, 56, and 60 in the tangential, radial, and spanwise directions, respectively. More details of the CFD model are furnished in [4]. Further, a detailed summary of the wing geometrical and mechanical properties, flow properties, and relevant dimensionless numbers are available in the reference.

Figure 11.8 shows that the computational response of the thrust coefficient correlates well with that of

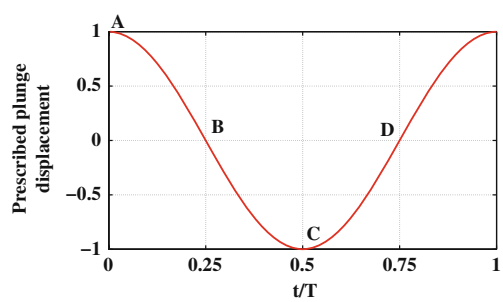

Fig. 11.7 Prescribed plunge motion for the rectangular wing (normalized w.r.t. amplitude) (Points A, B, C, and D are representative time instants corresponding to 0, $T/4$, $T/2$, and $3T/4$, respectively)

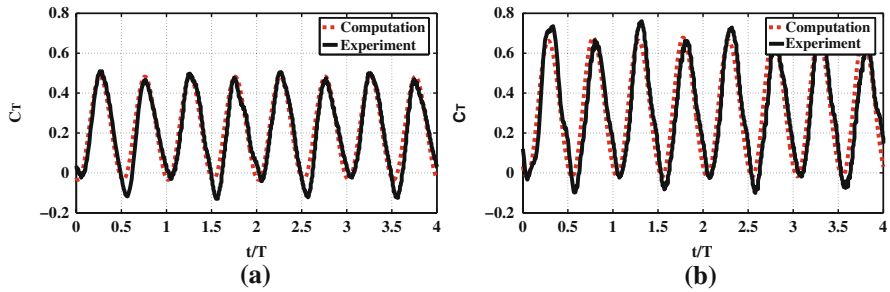

Fig. 11.8 Thrust coefficient as a function of time for rigid and flexible wings compared to experiment. (**a**) Rigid; (**b**) flexible [4]

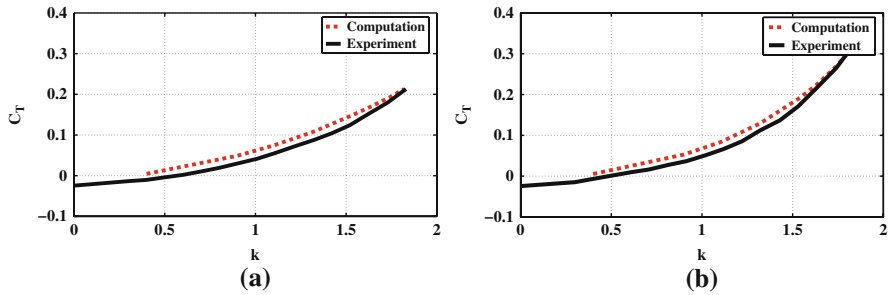

Fig. 11.9 Thrust coefficient as a function of reduced frequency. (**a**) Rigid; (**b**) flexible [4]

the experiment in both the rigid and the flexible wing cases. As seen from the figure, the frequency of the response is twice that of the plunging frequency as the maximum thrust occurs twice in a period as the wing passes through the neutral (zero) position (points B and D of Fig. 11.7). Also, the thrust coefficient of the flexible wing is greater than that of the rigid wing. This indicates that spanwise flexibility has a favorable impact on the thrust response in this case. It is worth noticing, however, that this result is not universal. The phase lag associated with structural flexibility alters the effective angles of attack, which means that the specific level and nature of flexibility can affect the outcome of thrust enhancement.

To assess the dependence of thrust production on the reduced frequency of oscillation, a parametric study was conducted on both the rigid and flexible wings. Figure 11.9 shows the computational results and their comparison with the experiment, showing good correlation between them. The thrust coefficient response increases gradually at low reduced frequencies and more rapidly at higher reduced frequencies. Figure 11.10 shows the variation of amplitude of tip displacement as a function of reduced frequency. Like the thrust coefficient, the displacements also increase with an increase in reduced frequency.

To better understand the implications of wing flexibility on the aerodynamics, detailed flow structure and pressure distributions need to be investigated. Results are shown for selected wing span locations and representative time instants on both the rigid and the flexible wings (see [4]).

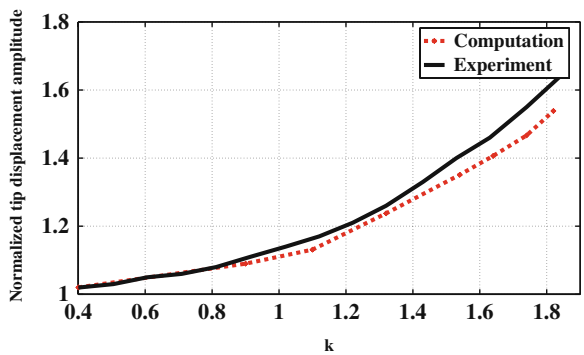

Fig. 11.10 Amplitude of tip displacement as a function of reduced frequency

Streamlines (as viewed from the reference frame moving with the prescribed motion) and pressure contours around the airfoil at 50% semi-span location are plotted for both rigid and flexible wings at four different time instants ($t = 0$ (A), $T/4$ (B), $T/2$ (C), and $3T/4$ (D) of Fig. 11.7) within a stroke period T. It may be observed from the figure that the streamlines in the case of the flexible wing hit the wing surface because the reference frame with respect to which they were plotted does not take into account the surface speed due to deformation.

The following features can be observed:

- At time $t = 0$, i.e., at the beginning of the downstroke, a vortex is seen on the bottom surface of the rigid wing close to the leading edge and a weaker one on the top surface close to the trailing edge. Conversely, in the case of the flexible wing, no vortex is seen on the top surface and the one on the bottom surface is stronger than its counterpart on the rigid wing.
- At time $t = T/4$, i.e., at the middle of the downstroke, in both rigid and flexible wings, the vortex on the bottom surface becomes weaker and moves downstream. Furthermore (only for the rigid wing) the smaller vortex on the top surface grows in size and also moves downstream toward the trailing edge. This is the point at which maximum thrust is generated in both the rigid and the flexible cases.
- At time $t = T/2$, i.e., at the beginning of the upstroke, in the case of the rigid wing, a large vortical structure is now seen on the top surface closer to the leading edge and a smaller-sized vortex on the bottom surface closer to the trailing edge. For the flexible wing, a much stronger vortex is seen on the top surface.
- At time $t = 3T/4$, in the case of the rigid wing, both the vortices seen at time $T/2$ become weaker and move toward the trailing edge. The vortex on the top surface moves downstream much less than the one on the bottom. In the flexible wing case, the weakening of the vortex is seen but it does not convect downstream as much as its counterpart on the rigid wing.

Figure 11.11 shows the time response of the instantaneous angle of attack for both rigid and flexible wings. The instantaneous effective angle of attack is defined as

$$\alpha_{inst} = tan^{-1}\left(\frac{-1}{U}\frac{dh(t)}{dt}\right)$$

where U is the wing velocity component normal to the uniform flow in the case of the rigid wing and in the case of the flexible wing, velocity due to elastic deformation is included as well. For the flexible wing case, two different stations along the semi-span (50 and 97%) are considered since each station sees a different effective angle of attack due to wing bending and spanwise variation of velocities induced due to deformation. As seen in the figure, the amplitude of the effective angle of attack in the case of the flexible wing (for 97% semi-span station) is at least 35% higher than that of the rigid wing. Angle of attack due to plunging of airfoils with leading-edge curvature promotes leading-edge suction. As seen

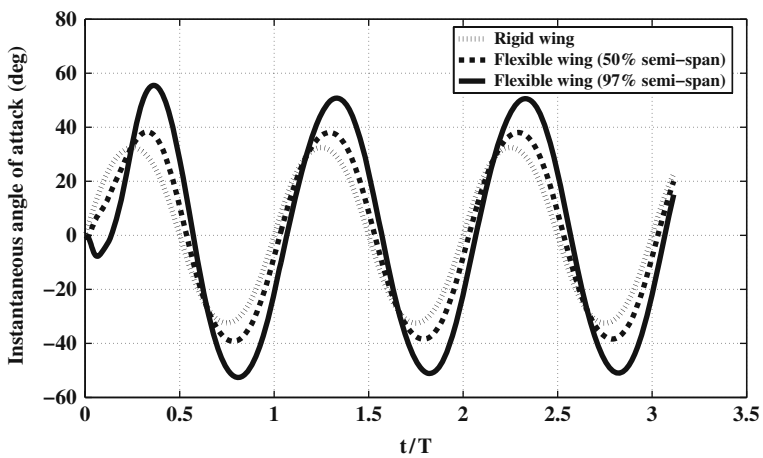

Fig. 11.11 Time response of the instantaneous angle of attack [4]

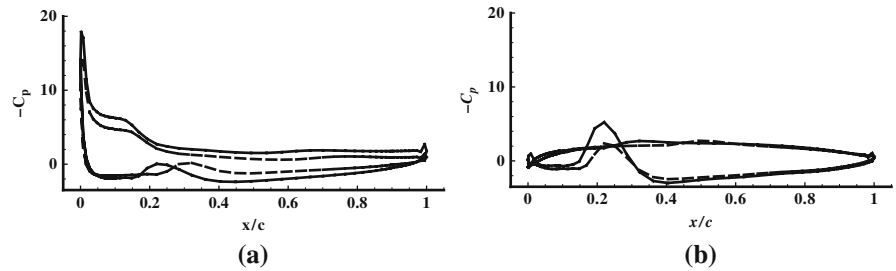

Fig. 11.12 Pressure distribution around 50% semi-span for two different time instants B and C of Fig. 11.7 (*dashed* – rigid, *solid* – flexible). (**a**) Time instant B; (**b**) time instant C [4]

from Fig. 11.11, structural flexibility has resulted in higher instantaneous effective angles of attack, which, in turn, promote larger streamline curvatures around the wing. From the momentum equations, streamline curvatures induce pressure gradients in corresponding manner. In order to understand the impact of this further, Fig. 11.12 shows the pressure field distributions at 50% semi-span station for two different time instants (points B and C in Fig. 11.7). It is seen in the figure that the effect of leading-edge suction is enhanced in the flexible wing case (higher suction peak near the leading edge) which helps explain the increase in thrust with increase in flexibility. This reinforces the fact shown in Fig. 11.8 that there is a thrust enhancement due to wing flexibility. Also, it is important to note here that flexible wings can yield favorable performance at quite high instantaneous angles of attack (50°) and large streamline curvatures without stalling.

11.5 Summary and Concluding Remarks

Fundamental understanding of interactions between structural flexibility and fluid flow is critical for the success of future MAV designs. Flexible wings may be beneficial for manmade flyers. Insects, bats, and birds stand as illuminating examples of utilizing flexibility along with unsteady aerodynamics for guiding research efforts in MAVs. Typical insect wings are characterized by membrane-like skin and a network of anisotropic veins to support the structure.

Membrane wings exhibit self-initiated vibration even in a steady free stream which lowers the effective angle of attack of the membrane structure compared to that of the rigid wing. To accurately simulate the mutual interaction between the flexible membrane structure and its surrounding viscous flow, coupled fluid and structure simulations are needed. Comparison of rigid, batten-reinforced, and perimeter-reinforced fixed-wing MAV designs shows that in the case of the rigid wing, the low Reynolds number (10^5) causes the laminar boundary layer to separate against the adverse pressure gradient at the wing root, and the low aspect ratio forces a strong wing tip vortex swirling system and leaves a low-pressure region at the wing tip. Whereas, in the case of the batten-reinforced wing, shape adaptation decreases the strength of the adverse pressure gradient, and thus the size of the separation bubble. In the case of the perimeter-reinforced wing, the interaction between the tip vortices and the longitudinal flow separation leads to unsteady vortex destabilization at high angles of attack. This was not seen in the rigid and the batten-reinforced cases.

Both experimental and computational investigations [4, 14] consistently indicated that within the range of appropriate non-dimensional parameters considered, span-wise flexibility can have a favorable impact on the thrust generation. Regarding fluid physics, leading-edge suction is important for thrust generation in flapping wings with leading-edge curvature. The structural flexibility results in higher instantaneous effective angles of attack. As long as the wing does not stall and the shape deformation does not cause the wing to experience out-of-phase movement from root to the tip, higher angles of attack promote larger streamline curvatures around the wing. From the momentum equations, streamline curvatures induce pressure gradients, resulting in enhanced leading-edge suction. Within the range of reduced frequencies considered (0.4–1.82), increasing reduced frequency enhances the thrust generated by both rigid and flexible wings.

Notwithstanding the fact that the case of a flexible wing with prescribed root plunge motion is

a very simplified representation of an actual insect wing structure envisioned for an MAV (the wing structures could be anisotropic, prescribed with three-dimensional flapping kinematics, of an elliptic planform, etc.), it highlights the importance of spanwise flexibility on thrust generation (one of the primary functions of flapping wings), the effective angle of attack, and the leading-edge suction at Strouhal numbers which fall within the range of those found in nature (0.2–0.4). Further, fundamental studies on canonical (simplified) flexible wing configurations are critical to the understanding of full-fledged flapping MAV aeroelasticity.

Observing the fast growth of papers and designs available in the open domain, it seems clear that strong attempts are being made in the research and development community to lay a foundation for the advancement of MAVs. While much progress has been made, more advancement is needed before we can develop robust and agile MAV technologies.

Acknowledgments This work was supported by the Air Force Office of Scientific Research's Multidisciplinary University Research Initiative (MURI) grant and by the Michigan/AFRL (Air Force Research Laboratory)/Boeing Collaborative Center in Aeronautical Sciences.

References

1. Archer, R., Sapuppo, J., Betteridge, D.: Propulsion characteristics of flapping wings. Aeronautical Journal **83**(825), 355–371 (1979)
2. Argentina, M., Mahadevan, L.: Fluid-flow-induced flutter of a flag. Proceedings of the National Academy of Science: Applied Mathematics **102**(6), 1829–1834 (2005)
3. Breugel V.F., Teoh, E.Z., Lipson, H.: A passively stable flapping hovering micro air vehicle. In: C. Ellington (ed.) Flying Insects and Robots. Springer-Verlag, Switzerland (2008)
4. Chimakurthi, S.K., Tang, J., Palacios, R., Cesnik, C., Shyy, W.: Computational aeroelasticity framework for analyzing flapping wing micro air vehicles. 49th AIAA/ASME/ASCE/AHS/ASC Structures, Structural Dynamics, and Materials Conference. AIAA Paper Number 2008-1814 Schaumburg, IL (2008)
5. Combes, S., Daniel, T.: Flexural stiffness in insect wings i. Scaling and the influence of wing venation. Journal of Experimental Biology **206**, 2979–2987 (2003)
6. Combes, S., Daniel, T.: Into thin air: Contributions of aerodynamic and inertial-elastic forces to wing bending in the hawkmoth manduca sexta. Journal of Experimental Biology **206**, 2999–3006 (2003)
7. Cubo, J., Casinos, A.: Mechanical properties and chemical composition of avian long bones. European Journal of Morphology **38**(2), 112–121 (2000)
8. DeLaurier, J., Harris, J.: Experimental study of oscillating-wing propulsion. Journal of Aircraft **19**(5), 368–373 (1982)
9. Frampton, K., Goldfarb, M., Monopoli, D., Cveticanin, D.: Passive aeroelastic tailoring for optimal flapping wings. In: T.J. Mueller (ed.) Fixed and Flapping Wing Aerodynamics for Micro Air Vehicle Applications, vol. 195, pp. 473–482. Progress in Astronautics and Aeronautics, AIAA New York (2001)
10. Freymuth, P.: Thrust generation by an airfoil in hover modes. Experiments in Fluids **9**(1–2), 17–24 (1990)
11. Galvao, R., Israeli, E., Song, A., Tian, X., Bishop, K., Swartz, S., Breuer, K.: The aerodynamics of compliant membrane wings modeled on mammalian flight mechanics. AIAA Paper Number 2006–2866 (2006).
12. Guglielmini, L., Blondeaux, P.: Propulsive efficiency of oscillating airfoils. European Journal of Mechanics B/Fluids **23**(2), 255–278 (2004)
13. Hamamoto, M., Ohta, Y., Hara, K., Hisada, T.: Application of fluid-structure interaction analysis to flapping flight of insects with deformable wings. Advanced Robotics **21**(1–2), 1–21 (2007)
14. Heathcote, S., Z., W., Gursul, I.: Effect of spanwise flexibility on flapping wing propulsion. Journal of Fluids and Structures **24**(2), 183–199 (2008)
15. Hepperle, M.: Aerodynamics of spar and rib structures. MH AeroTools Online Database, available at http://www.mh-aerotools.de/airfoils/ribs.htm, March 2007
16. Ifju, P., Jenkins, A., Ettingers, S., Lian, Y., Shyy, W.: Flexible-wing based micro air vehicles. IEEE Transactions on Robotics **22**, 137–146 (2002)
17. Jones K.D., Platzer, F.M.: Flow control using flapping wings for an efficient low-speed micro air vehicle. In: C. Ellington (ed.) Flying Insects and Robots. Springer-Verlag, Switzerland (2008)
18. Lian, Y.: Membrane and adaptively-shaped wings for micro air vehicles. Ph.D. thesis, Department of Mechanical and Aerospace Engineering, University of Florida, Gainsville, Florida (2003)
19. Lian, Y., Shyy, W.: Numerical simulations of membrane wing aerodynamics for micro air vehicle applications. Journal of Aircraft **42**(4), 865–873 (2005)
20. Lian, Y., Shyy, W.: Laminar-turbulent transition of a low Reynolds number rigid or flexible airfoil. AIAA Journal **45**(7), 1501–1513 (2007)
21. Lian, Y., Shyy, W., Viieru, D., Zhang, B.: Membrane wing aerodynamics for micro air vehicles. Progress in Aerospace Sciences **39**, 425–465 (2003)
22. Liani, E., Guo, S., Allegri, G.: Aeroelastic effect on flapping wing performance. 48th AIAA/ASME/ASCE/AHS/ASC Structures, Structural Dynamics, and Materials Conference. AIAA Paper Number 2007-2412 Honololu, Hawaii (2007)
23. Meirovitch, L.: Fundamentals of Vibrations. McGraw Hill, New York (2001)
24. Muniappan, A., Baskar, V., Duriyanandhan, V.: Lift and thrust characteristics of flapping wing micro air vehicle (mav). 43rd AIAA Aerospace Sciences Meeting and

Exhibit. AIAA Paper Number 2005-1055 Reno, Nevada (2005)
25. Ormiston, R.: Theoretical and experimental aerodynamics of the sail wing. Journal of Aircraft **8**(2), 77–84 (1971)
26. Sarkar, S., Venkatraman, K.: Numerical simulation of thrust generating flow past a pitching airfoil. Computers and Fluids **35**(1), 16–42 (2006)
27. Shimanuki, J., Machida, K.: Structure analysis of the wing of a dragonfly. Proceedings of the SPIE **5852**, 671–676 (2005)
28. Shyy, W., Berg, M., Ljungqvist, D.: Flapping and flexible wings for biological and micro air vehicles. Progress in Aerospace Sciences **35**(5), 455–505 (1999)
29. Shyy, W., Ifju, P., Viieru, D.: Membrane wing-based micro air vehicles. Applied Mechanics Reviews **58**(1–6), 283–301 (2005)
30. Shyy, W., Lian, Y., Tang, J., Liu, H., Trizila, B., Stanford, B., Bernal, L., Cesnik, C., Friedmann, P., Ifju, P.: Computational aerodynamics of low reynolds number plunging, pitching and flexible wings for mav applications. 46th AIAA Aerospace Sciences Meeting and Exhibit. AIAA Paper Number 2008-523 Reno, Nevada (2008)
31. Shyy, W., Lian, Y., Tang, J., Viieru, D., Liu, H.: Aerodynamics of Low Reynolds Number Flyers. Cambridge University Press (2008)
32. Singh, B.: Dynamics and aeroelasticity of hover capable flapping wings: Experiments and analysis. Ph.D. thesis, Department of Aerospace Engineering, University of Maryland, College Park, Maryland (2006)
33. Smith, M.J.C.: The effects of flexibility on the aerodynamics of moth wings: Towards the development of flapping-wing technology. 33rd AIAA Aerospace Sciences Meeting and Exhibit. AIAA Paper Number 1995-0743 Reno, Nevada (1995)
34. Song, A., Tian, X., Israeli, E., Galvo, R., Bishop, K., Swartz, S., Breuer, K.: The aero-mechanics of low aspect ratio compliant membrane wings, with applications to animal flight. 46th AIAA Aerospace Sciences Meeting and Exhibit. AIAA Paper Number 2008-517 Reno, Nevada (2008)
35. Stanford, B., Ifju, P.: Aeroelastic tailoring of fixed membrane wings for micro air vehicles. 49th AIAA/ASME/ASCE/AHS/ASC Structures, Structural Dynamics, and Materials Conference. AIAA Paper Number 2008-1790 Schaumburg, IL (2008)
36. Stanford, B., Sytsma, M., Albertani, R., Viieru, D., Shyy, W., Ifju, P.: Static aeroelastic model validation of membrane micro air vehicle wings. AIAA Journal **45**(12), 2828–2837 (2007)
37. Stanford B., I.P.A.R., Shyy, W.: Fixed membrane wings for micro air vehicles: Experimental characterization, numerical modeling, and tailoring. Progress in Aerospace Sciences **44**, 258–294 (2008)
38. Stults, J., Maple, R., Cobb, R., Parker, G.: Computational aeroelastic analysis of a micro air vehicle with experimentally determined modes. 23rd Applied Aerodynamics Conference. AIAA Paper Number 2005-4614 Toronto, Ontario, Canada (2005)
39. Tang, J., Chimakurthi, S.K., Palacios, R., Cesnik, C., Shyy, W.: Fluid-structure interactions of a deformable flapping wing for micro air vehicle applications. 46th AIAA Aerospace Sciences Meeting and Exhibit. AIAA Paper Number 2008-615 Reno, Nevada (2008)
40. Tang, J., Viieru, D., Shyy, W.: A study of aerodynamics of low reynolds number flexible airfoils. 37th AIAA Fluid Dynamics Conference and Exhibit. AIAA Paper Number 2007-4212 Miami, Florida (2007)
41. Tang, J., Zhu, K.: Numerical and experimental study of flow structure of low-aspect ratio wing. Journal of Aircraft **41**(5), 1196–1201 (2004)
42. Toomey, J., Eldredge, J.: Numerical and experimental investigation of the role of flexibility in flapping wing flight. 36th AIAA Fluid Dynamics Conference and Exhibit. AIAA Paper Number 2006-3211 San Francisco, California, USA (2006)
43. Waszak, R., Jenkins, N., Ifju, P.: Stability and control properties of an aeroelastic fixed wing micro aerial vehicle. AIAA Paper Number 2001-4005
44. Wills, D., Israeli, E., Persson, P., Drela, M., Peraire, J., Swartz, S.M., Breuer, K.S.: A computational framework for fluid structure interaction in biologically inspired flapping flight. 25th AIAA Applied Aerodynamics Conference. AIAA Paper Number 2007-3803 Miami, Florida (2007)
45. Wootton, J.: Support and deformability in insect wings. Journal of Zoology **193**, 447–468 (1981)
46. Wootton, R.: Springy shells, pliant plates, and minimal motors. abstracting the insect thorax to drive a micro air vehicle. In: C. Ellington (ed.) Flying Insects and Robots. Springer-Verlag, Switzerland (2008)
47. Zhu, Q.: Numerical simulation of a flapping foil with chordwise or spanwise flexibility. AIAA Journal **45**(10), 2448–2457 (2007)